Review Article



# Multimodality imaging of mediastinal masses and mimics

**John Matthew Archer, Jitesh Ahuja, Chad D. Strange, Girish S. Shroff, Gregory W. Gladish, Bradley S. Sabloff, Mylene T. Truong^**

Department of Thoracic Imaging, University of Texas MD Anderson Cancer Center, Houston, TX, USA

*Contributions:* (I) Conception and design: All authors; (II) Administrative support: All authors; (III) Provision of study materials or patients: All authors; (IV) Collection and assembly of data: All authors; (V) Data analysis and interpretation: All authors; (VI) Manuscript writing: All authors; (VII) Final approval of manuscript: All authors.

*Correspondence to:* Mylene T. Truong, MD. Department of Thoracic Imaging, University of Texas MD Anderson Cancer Center, 1400 Pressler Street, Unit 1478, Houston, TX 77030-4008, USA. Email: mtruong@mdanderson.org.

**Abstract:** A wide variety of neoplastic and nonneoplastic conditions occur in the mediastinum. Imaging plays a central role in the evaluation of mediastinal pathologies and their mimics. Localization of a mediastinal lesion to a compartment and characterization of morphology, density/signal intensity, enhancement, and mass effect on neighboring structures can help narrow the differentials. The International Thymic Malignancy Interest Group (ITMIG) established a cross-sectional imaging-derived and anatomy-based classification system for mediastinal compartments, comprising the prevascular (anterior), visceral (middle), and paravertebral (posterior) compartments. Cross-sectional imaging is integral in the evaluation of mediastinal lesions. Computed tomography (CT) and magnetic resonance imaging (MRI) are useful to characterize mediastinal lesions detected on radiography. Advantages of CT include its widespread availability, fast acquisition time, relatively low cost, and ability to detect calcium. Advantages of MRI include the lack of radiation exposure, superior soft tissue contrast resolution to detect invasion of the mass across tissue planes, including the chest wall and diaphragm, involvement of neurovascular structures, and the potential for dynamic sequences during free-breathing or cinematic cardiac gating to assess motion of the mass relative to adjacent structures. MRI is superior to CT in the differentiation of cystic from solid lesions and in the detection of fat to differentiate thymic hyperplasia from thymic malignancy.

**Keywords:** Mediastinal compartments; mediastinal mass; computed tomography (CT); magnetic resonance imaging (MRI)

Received: 15 November 2022; Accepted: 28 April 2023; Published online: 08 May 2023.
doi: 10.21037/med-22-53
**View this article at:** https://dx.doi.org/10.21037/med-22-53

## Introduction

A wide variety of neoplastic and nonneoplastic conditions occur in the mediastinum. While many mediastinal masses are incidentally detected on imaging, some are associated with nonspecific symptoms such as shortness of breath and chest discomfort. Cross-sectional imaging plays a central role in the evaluation of mediastinal pathologies and their mimics. Improvements in computed tomography (CT) and magnetic resonance imaging (MRI) have resulted in greater lesion characterization allowing radiologists to suggest limited differentials or specific diagnoses.

## Mediastinal compartments classification

Several mediastinal classification systems have been developed, which historically were based on nonanatomic

^ ORCID: 0000-0001-9795-529X.

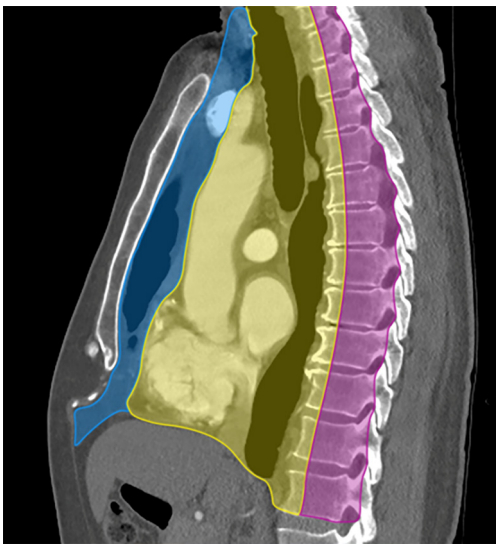

**Figure 1** ITMIG classification of mediastinal compartments bound superiorly by the thoracic inlet and inferiorly by the diaphragm. Sagittal CT with intravenous contrast shows the prevascular compartment (blue), bound anteriorly by the sternum and posteriorly by the anterior aspect of the parietal pericardium, and contains the thymus, fat, lymph nodes, and the left brachiocephalic vein. The visceral compartment (yellow) is bound anteriorly by the posterior boundaries of the prevascular compartment, and posteriorly by a vertical line 1 cm posterior to the anterior margin of each thoracic vertebral body, and contains the trachea, esophagus, lymph nodes, and vascular structures including the heart, thoracic aorta, superior vena cava, intrapericardial pulmonary arteries, and the thoracic duct. The paravertebral compartment (pink) is bound anteriorly by the posterior boundaries of the visceral compartment, and posterolaterally by a vertical line against the posterior margin of the chest wall at the lateral margin of the transverse process of the thoracic spine. ITMIG, International Thymic Malignancy Interest Group; CT, computed tomography.

divisions on the lateral chest radiographs. The International Thymic Malignancy Interest Group (ITMIG) established a cross-sectional imaging-derived and anatomy-based classification system for mediastinal compartments (1). The ITMIG classification system includes prevascular (anterior), visceral (middle), and paravertebral (posterior) compartments (2). Localization of a mediastinal lesion to a compartment can help narrow differentials (*Figure 1*).

### *Prevascular compartment*

The contents of the prevascular compartment include the thymus, lymph nodes, fat, and the left brachiocephalic vein. The prevascular compartment is bound superiorly by the thoracic inlet, inferiorly by the diaphragm, anteriorly by the sternum, laterally by the parietal mediastinal pleura, and posteriorly by the anterior aspect of the pericardium (2).

### *Visceral compartment*

The contents of the visceral compartment include the trachea, carina, esophagus, lymph nodes, and vascular structures such as the heart, thoracic aorta, superior vena cava (SVC), intrapericardial pulmonary arteries, and thoracic duct. The visceral compartment is bound superiorly by the thoracic inlet, inferiorly by the diaphragm, anteriorly by the posterior boundary of the prevascular compartment, and posteriorly by a vertical line connecting each thoracic vertebral body 1 cm posterior to its anterior margin (2).

### *Paravertebral compartment*

The contents of the paravertebral compartment include the thoracic spine and the paravertebral soft tissues. The paravertebral compartment is bound superiorly by the thoracic inlet, inferiorly by the diaphragm, anteriorly by the posterior boundary of the visceral compartment, and posterolaterally by a vertical line at the lateral margin of the transverse processes along the posterior margin of the chest wall (2).

## Imaging evaluation

Chest radiography can detect a mediastinal mass with the loss of normal mediastinal borders (referred to as the silhouette sign) (*Figure 2*). The American College of Radiology Appropriateness Criteria Imaging of Mediastinal Masses recommends either CT or MRI as the next imaging study of patients with indeterminate mediastinal mass detected on radiography (3). CT and MRI can characterize size, location, morphology, margins, density/intensity, enhancement, and invasion of neighboring structures (4). Advantages of CT include its widespread availability, fast acquisition time, relatively low cost, and detection of calcium (5). Advantages of MRI include lack of radiation exposure, superior soft tissue contrast resolution to detect invasion of the mass across tissue planes, including the chest wall and diaphragm, involvement of neurovascular structures, and potential for dynamic sequences during free-

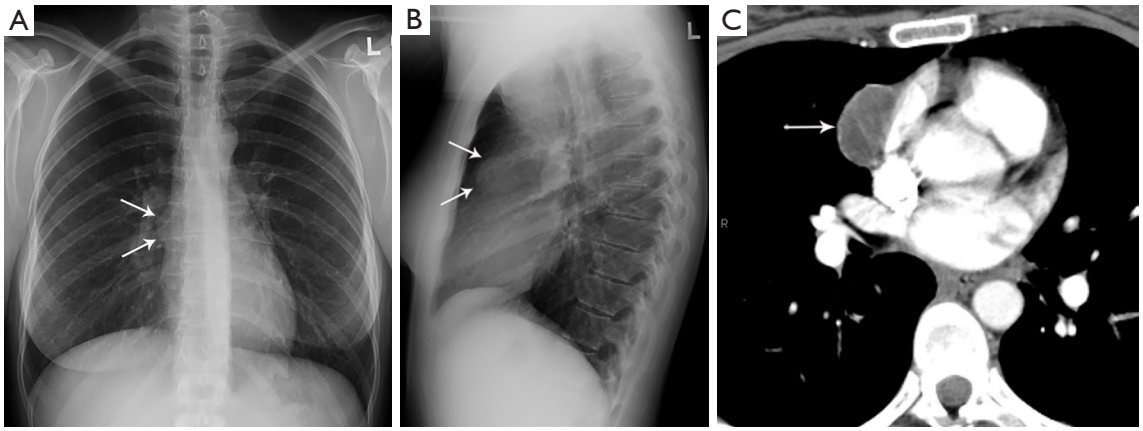


**Figure 2** Pericardial cyst. (A,B) Frontal and lateral chest radiograph shows subtle contour abnormality (arrows) with loss of the silhouette of part of the right mediastinal border termed the "silhouette sign". (C) CT shows low attenuation consistent with pericardial cyst (arrow). CT, computed tomography.

breathing or cinematic cardiac gating to assess motion of the mass relative to adjacent structures (3). MRI is superior to CT in the differentiation of cystic from solid lesions and in detection of fat to differentiate thymic hyperplasia from thymic malignancy.

## Cystic lesions

Cystic lesions represent 15% to 20% of mediastinal masses (6). Cystic lesions occur in all three mediastinal compartments. CT features that distinguish benign cysts include an imperceptible or thin wall with no significant enhancement, homogenous attenuation, water attenuation [between 0 and 10 Hounsfield units (HU)], and no invasion of mediastinal structures (7). However, some benign mediastinal cysts can have attenuation values of up to 100 HU and therefore mimic solid lesions on CT, leading to unnecessary surgical resection, including thymectomy (8).

When CT features are indeterminate, further imaging evaluation with MRI can provide diagnostic information (9). Cysts on MRI typically are hypointense on T1-weighted images, hyperintense on T2-weighted images and do not show contrast enhancement. However, cysts with blood products can be hypointense on T2-weighted MRI.

### *Pericardial cyst*

Pericardial cysts are most commonly located in the anterior cardiophrenic angles, right more common than left (10). However, these lesions can arise anywhere along the pericardial lining and can be remote from the cardiophrenic angles (10) (*Figure 3*). Approximately one-third of pericardial cysts are associated with symptoms including chest pain, dyspnea, or persistent cough (10). Pedunculated pericardial cysts can appear to be mobile when imaged at different times (11). On radiography pericardial cysts appear as smooth, round masses at the cardiophrenic angle. On CT, these lesions demonstrate water attenuation and an imperceptible wall.

### *Bronchogenic cyst*

Bronchogenic cysts develop from abnormal budding of the primitive ventral foregut, which gives rise to the tracheobronchial tree (12). Bronchogenic cysts contain mucoid material and a respiratory epithelium lining (13).

In one series of 66 patients, 58% were symptomatic at presentation with the most common symptoms being pain, dyspnea, respiratory infection, wheezing, and cough (14). Although these lesions most commonly are located in the mediastinum, approximately 15% of bronchogenic cysts are extramediastinal, located in the lung parenchyma or rarely in the diaphragm or pleura (14).

These lesions have variable appearances on CT and MRI, depending on their contents. On CT, characteristic findings include sharp margins with soft-tissue or water attenuation (14). On MRI, these lesions can demonstrate variable signal intensity on T1-weighted sequences depending on the composition on their contents, with approximately 50% hyperintense relative to skeletal muscle (14). On T2-

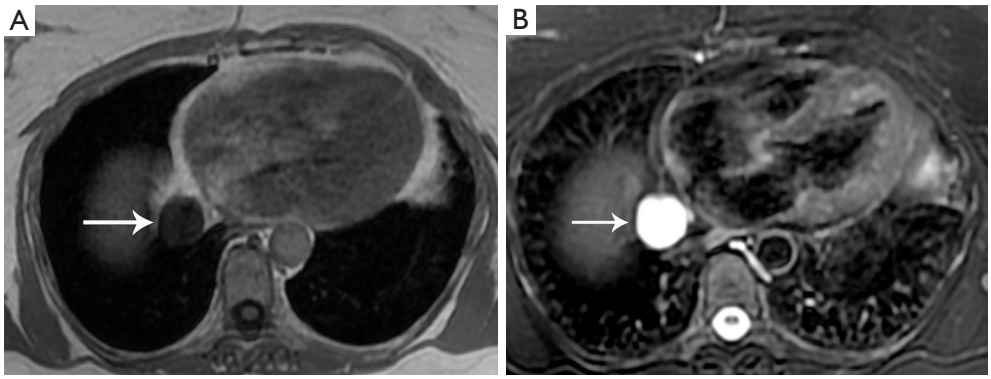


**Figure 3** Pericardial cyst. (A,B) MRI images show typical low signal intensity on T1-weighted (A) and high signal intensity on T2-weighted (B) images of fluid (arrow) in the pericardial cyst. MRI, magnetic resonance imaging.

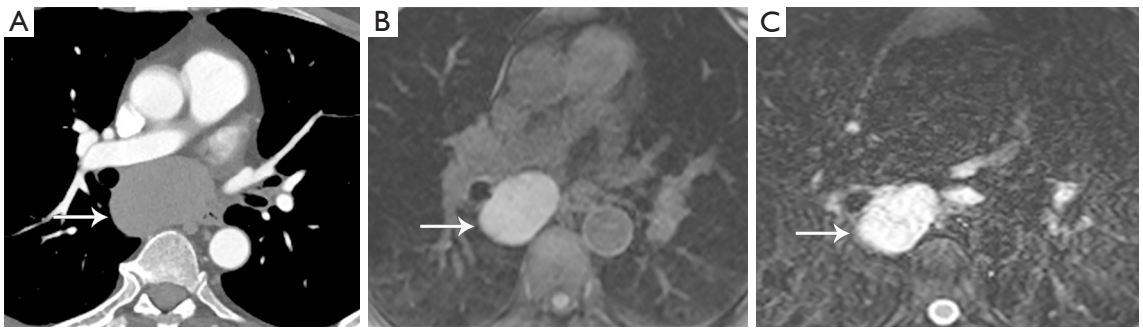


**Figure 4** Esophageal duplication cyst. (A) Contrast enhanced CT shows lesion (arrow) in the right subcarinal region with heterogeneous attenuation and could be cystic or solid. When CT is indeterminate, MRI is useful to differentiate fluid from solid mediastinal lesions. (B,C) MRI images show the visceral mediastinal lesion (arrow) with intermediate signal intensity on T1-weighted (B) and high signal intensity on T2-weighted (C) MRI images. The intermediate signal intensity on T1-weighted images can be seen with cysts with proteinaceous material. CT, computed tomography; MRI, magnetic resonance imaging.

weighted sequences, bronchogenic cysts are isointense to hyperintense relative to cerebrospinal fluid (13,14).

### *Duplication cyst*

Esophageal duplication cysts are the second most common benign esophageal lesion, with a wall comprised of smooth muscle and a mucosal lining (12,15). Ectopic gastric mucosa may be present within these lesions, which can result in hemorrhage or ulceration (2). Esophageal duplication cysts are typically located adjacent to or within the esophageal wall and can have thick walls (7). Similar to other mediastinal cystic lesions, the CT and MRI appearance can be variable depending on the cyst contents. Proteinaceous or hemorrhagic contents can cause these lesions to have hyperintense signal on T1-weighted sequences and soft-tissue attenuation on CT (*Figure 4*).

## Fat-containing lesions

Fat-containing mediastinal lesions include both benign and malignant processes, such as mature teratoma, thymolipoma, thymic hyperplasia, lipoma, liposarcoma, and fat necrosis. On CT, fat-containing mediastinal lesions demonstrate macroscopic fat measuring between –40 and –120 HU. On MRI, areas of macroscopic fat demonstrate hyperintense signal on T1-weighted images and loss of signal of signal on T1-weighted fat saturated images. In-phase and opposed-phase gradient echo sequences can be helpful identifying intravoxel fat. When fat and soft tissue are present in the same voxel, as typically present with thymic hyperplasia or the normal thymus, there is a homogeneous decrease in signal intensity on opposed-phase images compared to in-phase images. When this signal drop is not clearly visible to the naked eye, quantitative calculation of signal drop in

chemical shift MRI can be useful. This can be measured with the Chemical Shift Ratio (CSR) or the more recent Signal Intensity Index (SII) (16). The CSR is dependent on the signal intensity of paraspinal musculature and its formula is: CSR = (tSIop/mSIop)/(tSIin/mSIin). On the other hand, SII does not depend on muscle signal intensity and is calculated as: SIIthy = [(tSIin – tSIop)/(tSIin)] × 100% (17), where t = thymus, SI = signal intensity, m = muscle, op = opposed phase, in = in phase.

**Figure 5** Mature teratoma. Contrast enhanced CT shows large right mediastinal mass with heterogeneous attenuation, including calcifications (long arrow) and fat (short arrows). There is mass effect on the right atrium. CT, computed tomography.

### *Mature teratoma*

Mature teratomas are benign mediastinal germ cell tumors, typically containing fat, fluid, calcification, and soft tissue (18). In a series of 66 mediastinal mature teratomas evaluated with CT, soft tissue was observed in 100%, fluid in 88%, fat in 76%, and calcifications in 53% (19) (*Figure 5*). Mature teratomas are more common in young patients, accounting for approximately 25% of anterior mediastinal masses in ages 10 to 19 and less than 5% over age 50 (20).

At CT, mature teratomas characteristically have a well-defined, lobulated, smooth margin with a heterogenous appearance (21). Common MRI findings include areas of hyperintense signal on T2-weighted sequences (consistent with fluid), and areas of hyperintense signal on T1-weighted sequences that are hypointense on fat-suppressed sequences (19).

### *Fat necrosis*

Mediastinal fat necrosis is a rare, self-limiting process that can occur following trauma, interventional procedures, or surgery. On CT, characteristic findings include fat attenuation surrounded by a rim of soft tissue, with areas of fat stranding (22). On positron emission tomography (PET)/CT, fat necrosis can show focal avid uptake of [18F]-fluoro-2-deoxy-D-glucose (FDG) (23) (*Figure 6*). The CT and PET findings can present a diagnostic dilemma, as they can mimic nodal metastases. Partial or complete resolution of

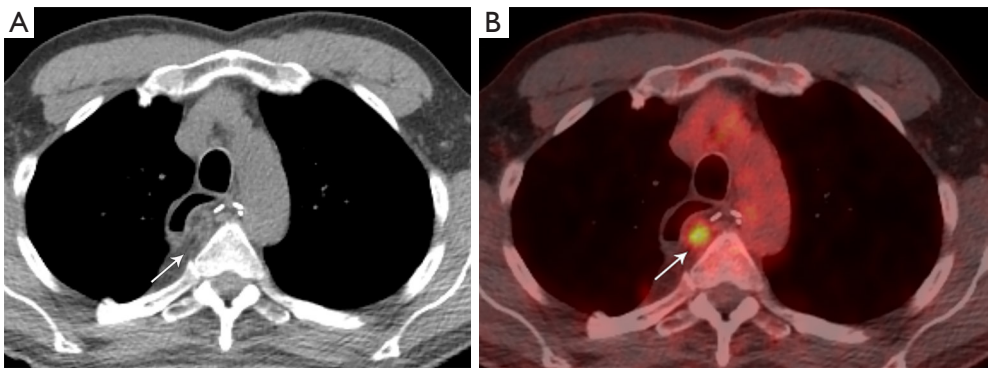


**Figure 6** Fat necrosis. (A) CT shows oval lesion (arrow) posterior to the gastric pull-through in a patient treated for esophageal cancer. The lesion shows predominant fat attenuation demarcated by a soft tissue rim, typical of fat necrosis. (B) FDG PET/CT shows the fat necrosis (arrow) is FDG avid due to the inflammatory component and can be misinterpreted as tumor recurrence. CT, computed tomography; FDG, fluoro-2-deoxy-D-glucose; PET, positron emission tomography.

**Figure 7** Hemangioma. CT shows large left mediastinal mass with focus of calcification (arrow) consistent with phlebolith interspersed with soft tissue and fat. CT, computed tomography.

FDG uptake is expected on follow-up PET/CT (23).

Spontaneous necrosis of the juxtapericardial mediastinal fat is an uncommon condition, typically presenting as a well-circumscribed fatty lesion with adjacent inflammatory changes along the cardiophrenic angle in patients presenting with acute chest pain (24). This condition is typically self-limiting and treatment consists of supportive therapy such as nonsteroidal anti-inflammatory drugs.

## Enhancing lesions

### *Hemangioma*

Mediastinal hemangiomas are uncommon benign vascular tumors, accounting for less than 0.5% of mediastinal masses (25). These lesions are most commonly located in the prevascular and paravertebral compartments (25,26). Histologically, hemangiomas are composed of vascular spaces with various stromal tissues, including fat, myxoid and fibrous tissues (27). On CT, these lesions are well circumscribed, with smooth or lobulated margins and heterogeneous attenuation. Similar to extramediastinal hemangiomas, one pattern of enhancement is the discontinuous peripheral nodular enhancement with progressive fill-in on delayed phases on both CT and MRI (28). On MRI, hemangiomas are hyperintense on T2-weighted sequences. Calcified phleboliths may be present. Although uncommon, fat may be interspersed throughout these lesions (25,29) (*Figure* 7).

### *Esophageal leiomyoma*

Although leiomyomas are the most common benign neoplasm of the esophagus, esophageal carcinoma is approximately 50 times more common (15,30). While small tumors are typically asymptomatic, larger tumors can be associated with symptoms including epigastric discomfort, dysphagia, regurgitation, and gastrointestinal hemorrhage (30). These tumors occur most commonly in the middle and distal portions of the esophagus and multiple tumors are found in 3% to 10% of patients (30). On CT, leiomyomas are typically isoattenuating or hypoattenuating relative to smooth muscle on nonenhanced CT, with homogeneous enhancement following contrast administration (15,31). Calcifications may be present, and can be helpful in distinguishing them from other benign and malignant esophageal tumors (31). On MRI, leiomyomas are typically slightly hyperintense on T2-weighted sequences (15,31,32). Minimal or no FDG uptake is usually seen on PET (15,31).

### *Carney triad*

The association of gastrointestinal leiomyosarcoma, extra-adrenal paraganglioma, and pulmonary chondromas was first described in 1977 by J. Aidan Carney (33). Carney triad is a rare condition caused by the down-regulation of succinate dehydrogenase (34). Although termed a triad, adrenocortical tumors and esophageal leiomyoma have been associated with this condition more recently (35).

Tumors originating from chromaffin cells are located in 90% of cases in the adrenal gland and called pheochromocytomas, while in the remaining 10% of cases have an extra-adrenal origin (paraganglionic cells scattered throughout the body) and are termed paragangliomas (36). In the anterior mediastinum, paragangliomas arise from the parasympathetic paraganglia, usually the aortic body chemoreceptors located in the aorticopulmonary window, and are termed aorticopulmonary paragangliomas or aortic body tumors. In the posterior mediastinum, paragangliomas arise from the sympathetic chain along the neck of the ribs in the paravertebral sulci. Mediastinal paragangliomas have indistinguishable imaging characteristics to paragangliomas elsewhere in the body. On CT, paragangliomas may show calcifications, areas of low attenuation that can reflect hemorrhage or cystic degeneration, and intense enhancement following the administration of contrast (36) (*Figure 8*). On MRI, paragangliomas are typically hyperintense on T2-weighted sequences and have a characteristic "salt-and-pepper" pattern cause by areas of signal void related to high velocity flow in intratumoral vessels (36). However, many paragangliomas, especially

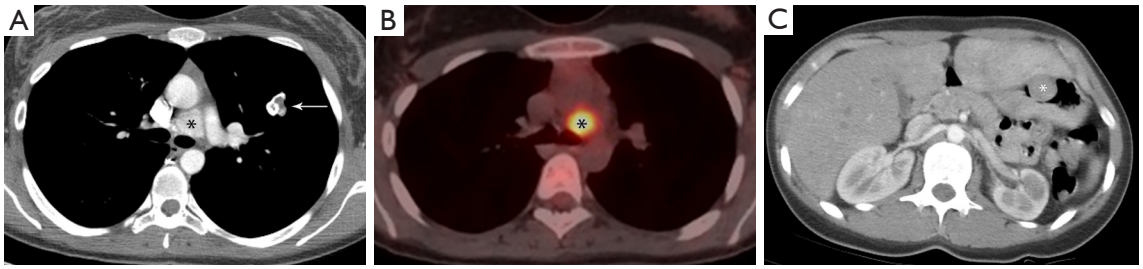


**Figure 8** Carney's triad. (A) Contrast enhanced CT shows enhancement of the left paratracheal mediastinal soft tissue mass (asterisk) due to paraganglioma and a solid lung nodule in the left upper lobe with coarse calcification (arrow) consistent with chondroma. (B) FDG PET/CT shows increased FDG uptake of the paraganglioma (asterisk). (C) Contrast-enhanced CT abdomen shows round well-circumscribed soft tissue nodule (asterisk) in the anterior wall of the stomach consistent with gastrointestinal stromal tumor. CT, computed tomography; FDG, fluoro-2-deoxy-D-glucose; PET, positron emission tomography.

small ones, may not exhibit the "salt and pepper pattern" on MRI. PET/CT with 68-Ga DOTATATE is increasingly used for the diagnosis and follow-up of paragangliomas. PET/CT with $^{18}$F-FDG has been shown to better detect metastatic disease/recurrent disease in comparison to 123-Iodine metaiodobenzylguanidine (MIBG) and CT/MRI (37).

Gastrointestinal stromal tumors (GIST) are the most common mesenchymal malignancy of the gastrointestinal tract (38). GISTs were previously referred to as gastrointestinal smooth muscle tumor: leiomyoma if benign, and leiomyosarcoma if malignant (38). While the stomach is the most common site of involvement, GISTs can occur from the distal esophagus to the anus (38). In the esophagus, the most common benign neoplasm is leiomyoma, far more common than GISTs. These lesions can present with gastrointestinal hemorrhage or pain. Distant metastases are present in greater than 50% of patients, with the peritoneum and liver being the most common sites of spread (39). While thoracic metastases are relatively uncommon, occurring in approximately 10% of patients, the most common sites of involvement are the lungs, intrathoracic lymph nodes, bones, and pleura (39). On CT, GISTs typical imaging characteristics include large, exophytic, heterogeneously enhancing masses with areas of hypo-enhancement corresponding to necrosis, hemorrhage, or cystic degeneration (40). On MRI, small GISTs (≤5 cm) appeared as round tumors with strong and homogeneous arterial enhancement and a persistent enhancement pattern. Large GISTs (>5 cm) appeared as lobulated tumors with mild heterogeneous gradual enhancement, and they frequently exhibited intratumoral cystic change. The presence of intratumoral cysts or a low apparent diffusion coefficient (ADC) value is suggestive of a high-risk GIST (41).

The final component of Carney's triad is pulmonary chondromas, composed of hyaline cartilage surrounded by a thin fibrous pseudocapsule (42). On CT, pulmonary chondromas typically appears as round nodules with smooth margins, and a variable amount of calcification (43). On MRI, calcifications within the lesions appear as foci of low signal intensity (44).

### *Ectopic parathyroid adenoma*

The parathyroid glands are typically located along the posterior border of the thyroid gland. Parathyroid glands located above or below the thyroid gland in the neck or mediastinum are considered ectopic (45). The inferior parathyroid glands are more commonly ectopic, located in the mediastinum in approximately 4% to 5% of the population (45). Patients can present with incidentally detected hypercalcemia (46). Symptoms of hypercalcemia can include muscle pain, lethargy, nausea, constipation, and confusion.

Parathyroid adenomas are typically oval or rounded with smooth margins, occasionally cystic (47). There are multiple options for imaging of parathyroid adenomas, including CT, MRI, and single photon emission computed tomography (SPECT) using technetium-99m (99mTc) sestamibi. Many centers utilize pre-contrast and post-contrast CT (with arterial and delayed phases) for the detection of parathyroid adenoma. The primary purpose of the pre-contrast CT is to distinguish high-attenuation thyroid tissue from arterially enhancing parathyroid adenoma (which should be low attenuation on pre-contrast images) (47) (*Figure 9*). Rapid washout of contrast material is expected from the arterial

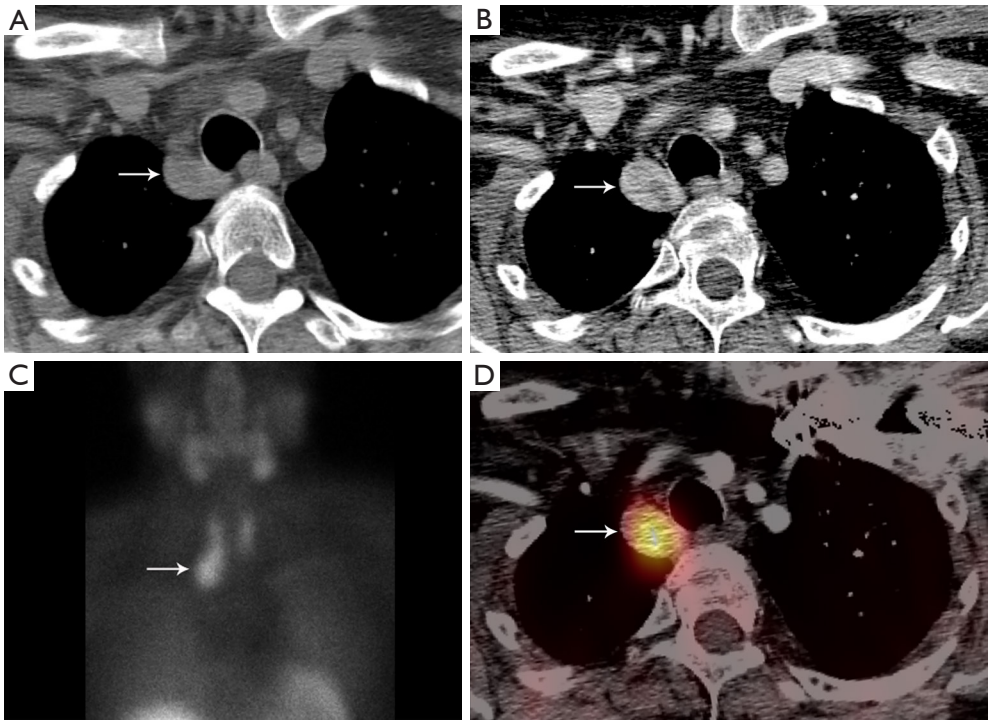


**Figure 9** Ectopic parathyroid adenoma. (A,B) Pre- and post-contrast enhanced CT show right paratracheal solid lesion (arrow) with heterogeneous enhancement. The pre-contrast CT is useful to differentiate high attenuation thyroid tissue from low attenuation parathyroid tissue. (C,D) Technetium-99m sestamibi parathyroid scintigraphy and SPECT/CT show the right parathyroid adenoma is sestamibi avid (arrow). CT, computed tomography; SPECT, single photon emission computed tomography.

to delayed phases (47). High-temporal-resolution dynamic contrast enhanced (DCE) MRI allows differentiation of the parathyroid glands from lymph nodes and thyroid tissue due to their faster arterial enhancement and earlier contrast washout, with a mean parathyroid maximal enhancement of 13 seconds earlier than thyroid tissue and 29 seconds earlier than lymph nodes using this technique (48). MRI has the benefit of making the diagnosis without subjecting the patient to ionizing radiation exposure.

Although the majority of parathyroid adenomas occur in isolation, several genetic syndromes have been associated with parathyroid neoplasia, including multiple endocrine neoplasia (MEN) types 1 and 2A. MEN 1 and 2A are autosomal dominant conditions (49). Hyperparathyroidism in these conditions is typically multiglandular (49). The classic components of MEN 1 include parathyroid tumors, pancreatic islet cell tumors, and pituitary tumors. Additional associations in MEN 1 include facial angiofibromas, adrenal cortical tumors, lipomas, and carcinoid tumors (49). MEN 2A is characterized by medullary thyroid carcinoma, pheochromocytomas, and parathyroid hyperplasia or tumors.

## Paravertebral lesions

The paravertebral compartment of the mediastinum includes the spine and paravertebral soft tissues. When a mass is detected in the paravertebral region on CT, the most likely diagnosis is a neurogenic lesion. There are two broad categories of neurogenic neoplasms: peripheral nerve sheath tumors such as schwannoma or neurofibroma which present as round or dumbbell lesions and the sympathetic ganglion neoplasms such as ganglioneuroma (*Figure 10*), ganglioneuroblastoma and neuroblastoma which present as

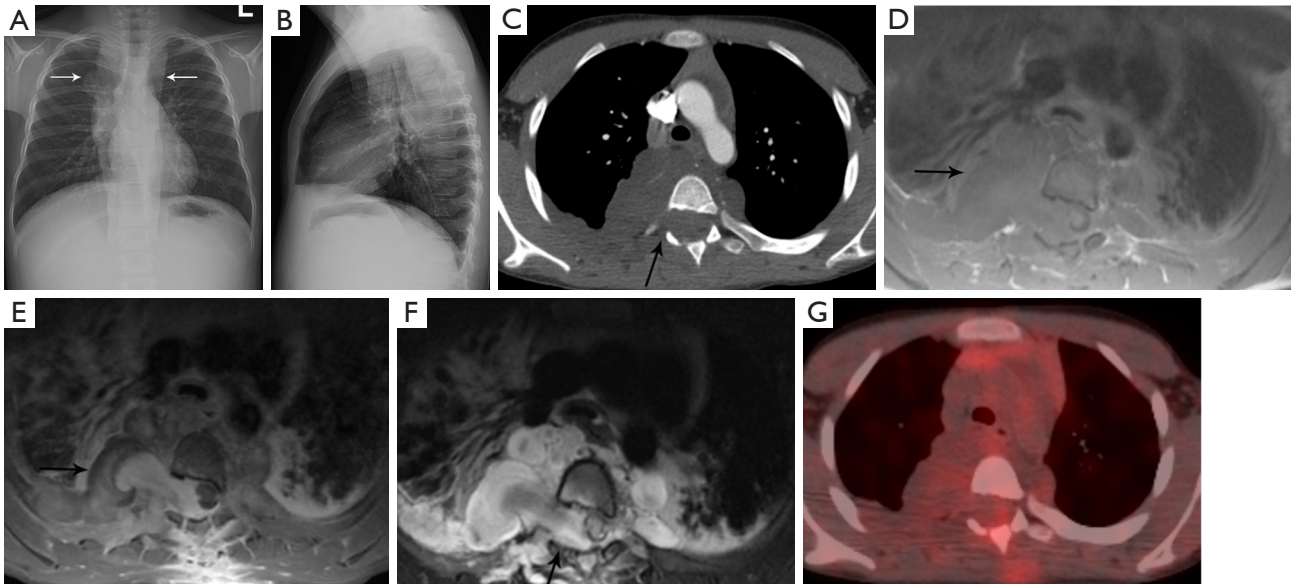


**Figure 10** Ganglioneuroma. (A,B) PA and lateral chest radiographs show elongated bilateral posterior mediastinal lesion (arrows) extending from the neck down to below the diaphragm. (C) Axial contrast enhanced CT shows bilateral paraspinal masses with low attenuation and enlargement of the right neural foramen of T4 (arrow) with extension into the spinal canal. (D) Axial T1-weighted MRI shows the mass (arrow) is heterogeneous with iso- to hyperintense signal. Extension into the spinal canal displaces and the spinal cord to the left with abnormal signal intensity within the cord due to cord compression and edema. (E) Axial T1-weighted post-contrast MRI shows the mass (arrow) enhances heterogeneously. (F) Axial T2-weighted MRI shows the mass (arrow) is heterogeneously hyperintense. (G) Fused PET/CT shows the ganglioneuroma is not FDG avid. Biopsy confirmed ganglioneuroma. PA, posterior anterior; CT, computed tomography; MRI, magnetic resonance imaging; PET, positron emission tomography; FDG, fluoro-2-deoxy-D-glucose.

elongated masses involving 3 or more vertebral levels. Other less common neoplasms in the differential include lymphoma, bone tumors, and metastases. Nonneoplastic entities include spinal infections, cystic lesions (meningocele and neurenteric cyst), pancreatic pseudocyst and extramedullary hematopoiesis.

Accounting for 70% of mediastinal neurogenic tumors, peripheral nerve sheath tumors arise from spinal or proximal intercostal nerves, less commonly from the vagus, recurrent laryngeal, or phrenic nerves (50). Peripheral nerve sheath neoplasms can show communication with the spinal canal. Areas of heterogeneity may be due to cystic changes or hemorrhage and are more common in schwannomas than in neurofibromas (*Figure 11*) (50). Neurogenic tumors can erode adjacent ribs or vertebrae and enlarge the neural foramina. MRI is useful to show the extent of intraspinal/extradural extension. The "fascicular sign" is seen in some schwannomas and refers to multiple hypointense, small, ring-like structures corresponding to fascicular bundles. The "target sign" is more commonly seen in neurofibromas than in schwannomas and refers to the central low signal intensity surrounded by peripheral high signal intensity. FDG PET/CT is useful to differentiate malignant peripheral nerve sheath tumors from benign neurofibromas, with sensitivity of 95% and specificity of 72% (51). It is important to be aware that some schwannomas may demonstrate intense FDG avidity (52).

## Additional imaging considerations for mediastinal lesions

Mediastinal lesions can exert mass effect on the critical

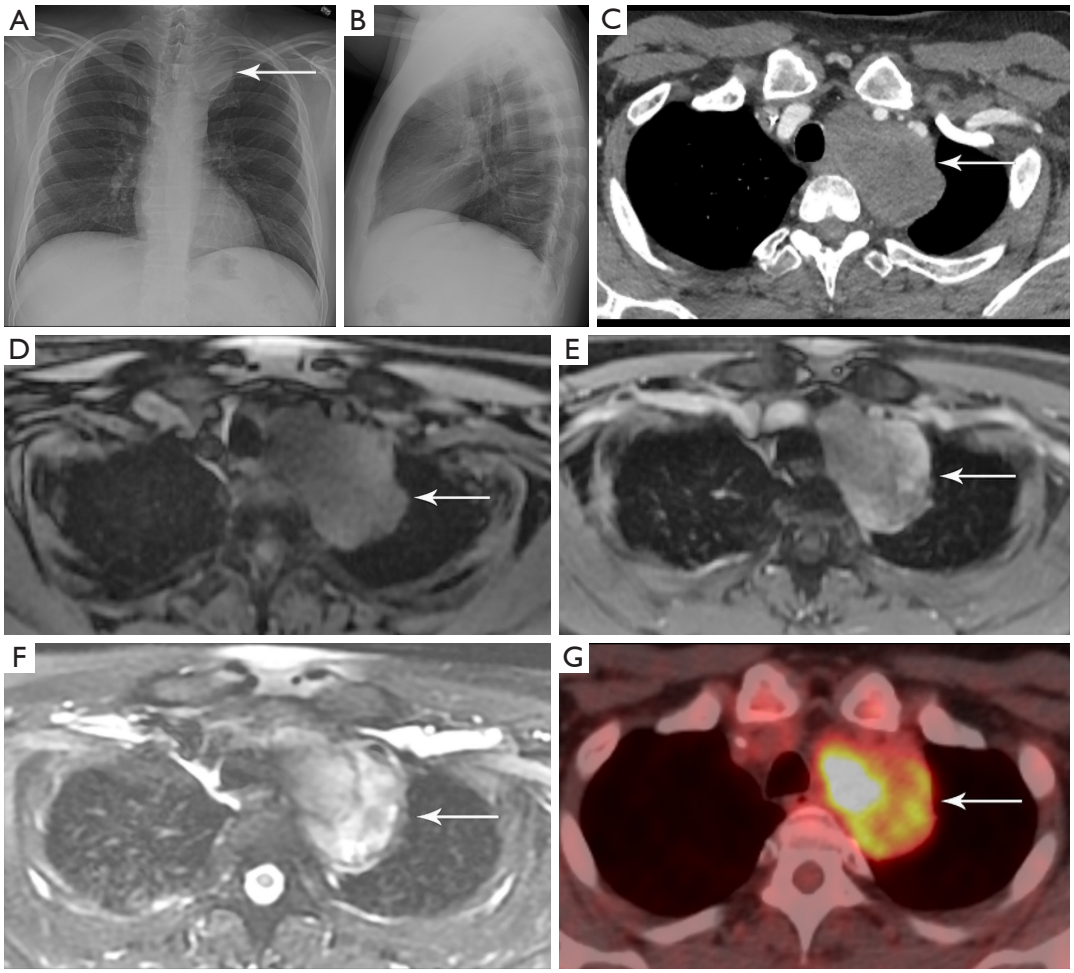


**Figure 11** Schwannoma. (A,B) PA and lateral chest radiographs show a left mediastinal mass (arrow) in the upper thorax. (C) Axial contrast enhanced CT shows the mass (arrow) is solid with heterogeneous attenuation. (D) Axial T1-weighted MRI shows the mass (arrow) is isointense to muscle. (E) Axial T1-weighted post-contrast MRI shows the mass (arrow) enhances heterogeneously. (F) Axial T2-weighted MRI shows the mass (arrow) is heterogeneously hyperintense with cystic areas. (G) Fused PET/CT shows the mass (arrow) is FDG avid. Biopsy confirmed schwannoma. PA, posterior anterior; CT, computed tomography; MRI, magnetic resonance imaging; PET, positron emission tomography; FDG, fluoro-2-deoxy-D-glucose.

vascular structures. Masses in the prevascular and visceral compartments can compress and obstruct the SVC. Patients with SVC obstruction may present with upper body edema, distended neck veins, dyspnea, cough, hoarseness, syncope, headaches, and dizziness (53). Cerebral edema and narrowing of the respiratory tract due to edema are rare, but potentially serious effects (53). The most common malignancies associated with SVC syndrome include lung cancer, lymphoma, metastatic cancer, germ-cell tumors, and thymomas (53). The imaging modality of choice is contrast enhanced CT (*Figure 12*). Symptoms may improve with treatment or as collateral circulation develops.

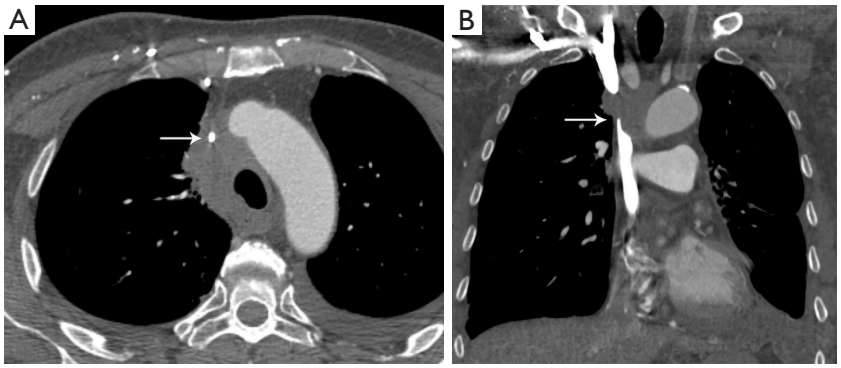


**Figure 12** SVC obstruction. (A) Axial contrast enhanced CT shows mediastinal adenopathy due to lung cancer narrowing the SVC (arrow) with multiple collaterals in the right anterior chest wall. (B) Coronal contrast enhanced CT shows the SVC is patent below the level of obstruction due to the adenopathy (arrow). SVC, superior vena cava; CT, computed tomography.

## Conclusions

Cross-sectional imaging with CT and MRI is indispensable in the evaluation of mediastinal pathologies. Localization of a mediastinal lesion to a compartment and characterization of morphology, density/intensity, enhancement, and mass effect on neighboring structures can help narrow differentials.

## Acknowledgments

The authors wish to thank Chastity A. Holmes, Executive Assistant in the Department of Thoracic Imaging at the University of Texas M.D. Anderson Cancer Center, for her invaluable help in manuscript preparation and Kelly M. Kage, Medical Illustrator in the Division of Diagnostic Imaging at the University of Texas M.D. Anderson Cancer Center for her skillful expertise in preparation of the figures for publication.
*Funding:* None.

## Footnote

*Peer Review File:* Available at https://med.amegroups.com/article/view/10.21037/med-22-53/prf

*Conflicts of Interest:* All authors have completed the ICMJE uniform disclosure form (available at https://med.amegroups.com/article/view/10.21037/med-22-53/coif). The authors have no conflicts of interest to declare.

*Ethical Statement:* The authors are accountable for all aspects of the work in ensuring that questions related to the accuracy or integrity of any part of the work are appropriately investigated and resolved.



## References

1. Carter BW, Tomiyama N, Bhora FY, et al. A modern definition of mediastinal compartments. J Thorac Oncol 2014;9:S97-101.
2. Carter BW, Benveniste MF, Madan R, et al. ITMIG Classification of Mediastinal Compartments and Multidisciplinary Approach to Mediastinal Masses. Radiographics 2017;37:413-36.
3. Expert Panel on Thoracic Imaging; Ackman JB, Chung JH, et al. ACR Appropriateness Criteria® Imaging of Mediastinal Masses. J Am Coll Radiol 2021;18:S37-S51.
4. Carter BW, Okumura M, Detterbeck FC, et al. Approaching the patient with an anterior mediastinal mass: a guide for radiologists. J Thorac Oncol 2014;9:S110-8.
5. Heeger AP, Ackman JB. Added Value of Magnetic Resonance Imaging for the Evaluation of Mediastinal Lesions. Radiol Clin North Am 2021;59:251-77.

6. Oldham HN Jr. Mediastinal tumors and cysts. Ann Thorac Surg 1971;11:246-75.
7. Jeung MY, Gasser B, Gangi A, et al. Imaging of cystic masses of the mediastinum. Radiographics 2002;22 Spec No:S79-93.
8. Ackman JB, Verzosa S, Kovach AE, et al. High rate of unnecessary thymectomy and its cause. Can computed tomography distinguish thymoma, lymphoma, thymic hyperplasia, and thymic cysts? Eur J Radiol 2015;84:524-33.
9. Madan R, Ratanaprasatporn L, Ratanaprasatporn L, et al. Cystic mediastinal masses and the role of MRI. Clin Imaging 2018;50:68-77.
10. Feigin DS, Fenoglio JJ, McAllister HA, et al. Pericardial cysts. A radiologic-pathologic correlation and review. Radiology 1977;125:15-20.
11. Cramer JA, Mann H, Layfield LJ. AIRP Best Cases in Radiologic-Pathologic Correlation: Migrating Pericardial Cyst. RadioGraphics 2014;34:373-6.
12. Berrocal T, Madrid C, Novo S, et al. Congenital anomalies of the tracheobronchial tree, lung, and mediastinum: embryology, radiology, and pathology. Radiographics 2004;24:e17.
13. Goitein O, Truong MT, Bekker E, et al. Potential Pitfalls in Imaging of the Mediastinum. Radiol Clin North Am 2021;59:279-90.
14. McAdams HP, Kirejczyk WM, Rosado-de-Christenson ML, et al. Bronchogenic cyst: imaging features with clinical and histopathologic correlation. Radiology 2000;217:441-6.
15. Lewis RB, Mehrotra AK, Rodriguez P, et al. From the radiologic pathology archives: esophageal neoplasms: radiologic-pathologic correlation. Radiographics 2013;33:1083-108.
16. Priola AM, Priola SM, Ciccone G, et al. Differentiation of rebound and lymphoid thymic hyperplasia from anterior mediastinal tumors with dual-echo chemical-shift MR imaging in adulthood: reliability of the chemical-shift ratio and signal intensity index. Radiology 2015;274:238-49.
17. Raptis CA, McWilliams SR, Ratkowski KL, et al. Mediastinal and Pleural MR Imaging: Practical Approach for Daily Practice. Radiographics 2018;38:37-55.
18. Walker CM. Muller's imaging of the chest. 2nd edition. ed. Philadelphia, PA: Elsevier; 2018.
19. Moeller KH, Rosado-de-Christenson ML, Templeton PA. Mediastinal mature teratoma: imaging features. AJR Am J Roentgenol 1997;169:985-90.
20. Carter BW, Marom EM, Detterbeck FC. Approaching the patient with an anterior mediastinal mass: a guide for clinicians. J Thorac Oncol 2014;9:S102-9.
21. Gaerte SC, Meyer CA, Winer-Muram HT, et al. Fat-containing lesions of the chest. Radiographics 2002;22 Spec No:S61-78.
22. Shroff GS, Ahuja J, Strange CD, et al. Pitfalls in Oncologic Imaging of the Pericardium on CT and PET/CT. Semin Ultrasound CT MR 2022;43:194-203.
23. Kashyap R, Lau E, George A, et al. High FDG activity in focal fat necrosis: a pitfall in interpretation of posttreatment PET/CT in patients with non-Hodgkin lymphoma. Eur J Nucl Med Mol Imaging 2013;40:1330-6.
24. Gayer G. Mediastinal (Epipericardial) Fat Necrosis: An Overlooked and Little Known Cause of Acute Chest Pain Mimicking Acute Coronary Syndrome. Semin Ultrasound CT MR 2017;38:629-33.
25. McAdams HP, Rosado-de-Christenson ML, Moran CA. Mediastinal hemangioma: radiographic and CT features in 14 patients. Radiology 1994;193:399-402.
26. Yamazaki A, Miyamoto H, Saito Y, et al. Cavernous hemangioma of the anterior mediastinum: case report and 50-year review of Japanese cases. Jpn J Thorac Cardiovasc Surg 2006;54:221-4.
27. Cheung YC, Ng SH, Wan YL, et al. Dynamic CT features of mediastinal hemangioma: more information for evaluation. Clin Imaging 2000;24:276-8.
28. Li SM, Hsu HH, Lee SC, et al. Mediastinal hemangioma presenting with a characteristic feature on dynamic computed tomography images. J Thorac Dis 2017;9:E412-5.
29. Agarwal PP, Seely JM, Matzinger FR. Case 130: mediastinal hemangioma. Radiology 2008;246:634-7.
30. Mutrie CJ, Donahue DM, Wain JC, et al. Esophageal leiomyoma: a 40-year experience. Ann Thorac Surg 2005;79:1122-5.
31. Lichtenberger JP 3rd, Zeman MN, Dulberger AR, et al. Esophageal Neoplasms: Radiologic-Pathologic Correlation. Radiol Clin North Am 2021;59:205-17.
32. Yang PS, Lee KS, Lee SJ, et al. Esophageal leiomyoma: radiologic findings in 12 patients. Korean J Radiol 2001;2:132-7.
33. Carney JA, Sheps SG, Go VL, et al. The triad of gastric leiomyosarcoma, functioning extra-adrenal paraganglioma and pulmonary chondroma. N Engl J Med 1977;296:1517-8.
34. Settas N, Faucz FR, Stratakis CA. Succinate dehydrogenase (SDH) deficiency, Carney triad and the epigenome. Mol Cell Endocrinol 2018;469:107-11.
35. Benesch M, Wardelmann E, Ferrari A, et al.


 

Gastrointestinal stromal tumors (GIST) in children and adolescents: A comprehensive review of the current literature. Pediatr Blood Cancer 2009;53:1171-9.
36. Ocazionez D, Shroff GS, Vargas D, et al. Imaging of Intrathoracic Paragangliomas. Semin Ultrasound CT MR 2017;38:584-93.
37. Timmers HJ, Chen CC, Carrasquillo JA, et al. Staging and functional characterization of pheochromocytoma and paraganglioma by 18F-fluorodeoxyglucose (18F-FDG) positron emission tomography. J Natl Cancer Inst 2012;104:700-8.
38. Miettinen M, Lasota J. Gastrointestinal stromal tumors. Gastroenterol Clin North Am 2013;42:399-415.
39. Shinagare AB, Ip IK, Lacson R, et al. Gastrointestinal stromal tumor: optimizing the use of cross-sectional chest imaging during follow-up. Radiology 2015;274:395-404.
40. Hong X, Choi H, Loyer EM, et al. Gastrointestinal stromal tumor: role of CT in diagnosis and in response evaluation and surveillance after treatment with imatinib. Radiographics 2006;26:481-95.
41. Yu MH, Lee JM, Baek JH, et al. MRI features of gastrointestinal stromal tumors. AJR Am J Roentgenol 2014;203:980-91.
42. Chatzopoulos K, Johnson TF, Boland JM. Clinical, Radiologic, and Pathologic Characteristics of Pulmonary Hamartomas With Uncommon Presentation. Am J Clin Pathol 2021;155:903-11.
43. McGahan JP. Carney syndrome: usefulness of computed tomography in demonstrating pulmonary chondromas. J Comput Assist Tomogr 1983;7:137-9.
44. Sodhi KS, Ciet P, Vasanawala S, et al. Practical protocol for lung magnetic resonance imaging and common clinical indications. Pediatr Radiol 2022;52:295-311.
45. Eslamy HK, Ziessman HA. Parathyroid scintigraphy in patients with primary hyperparathyroidism: 99mTc sestamibi SPECT and SPECT/CT. Radiographics 2008;28:1461-76.
46. Cabral FC, Trotman-Dickenson B, Madan R. Hypervascular mediastinal masses: action points for radiologists. Eur J Radiol 2015;84:489-98.
47. Hoang JK, Sung WK, Bahl M, et al. How to perform parathyroid 4D CT: tips and traps for technique and interpretation. Radiology 2014;270:15-24.
48. Nael K, Hur J, Bauer A, et al. Dynamic 4D MRI for Characterization of Parathyroid Adenomas: Multiparametric Analysis. AJNR Am J Neuroradiol 2015;36:2147-52.
49. Scarsbrook AF, Thakker RV, Wass JA, et al. Multiple endocrine neoplasia: spectrum of radiologic appearances and discussion of a multitechnique imaging approach. Radiographics 2006;26:433-51.
50. Strollo DC, Rosado-de-Christenson ML, Jett JR. Primary mediastinal tumors: part II. Tumors of the middle and posterior mediastinum. Chest 1997;112:1344-57.
51. Bredella MA, Torriani M, Hornicek F, et al. Value of PET in the assessment of patients with neurofibromatosis type 1. AJR Am J Roentgenol 2007;189:928-35.
52. Broski SM, Johnson GB, Howe BM, et al. Evaluation of (18)F-FDG PET and MRI in differentiating benign and malignant peripheral nerve sheath tumors. Skeletal Radiol 2016;45:1097-105.
53. Wilson LD, Detterbeck FC, Yahalom J. Clinical practice. Superior vena cava syndrome with malignant causes. N Engl J Med 2007;356:1862-9.

doi: 10.21037/med-22-53
**Cite this article as:** Archer JM, Ahuja J, Strange CD, Shroff GS, Gladish GW, Sabloff BS, Truong MT. Multimodality imaging of mediastinal masses and mimics. Mediastinum 2023;7:27.